The impact of the nitrogen-to-oxygen ratio on ionized nebulae diagnostics based on [NII] emission lines.

Enrique Pérez-Montero[1,2] & Thierry Contini[2]

[1] *Instituto de Astrofísica de Andalucía, CSIC, Apdo. 3004, 18080, Granada, Spain.*
[2] *Laboratoire d'Astrophysique de Toulouse-Tarbes, Université de Toulouse, CNRS, 14, avenue Edouard Belin, F31400 Toulouse, France*

ABSTRACT
We study the relation between nitrogen and oxygen abundances as a function of metallicity for a sample of emission-line objects for which a direct measurement of the metallicity has been possible. This sample is representative of the very different conditions in ionization and chemical enrichment that we can find in the Universe. We first construct the N/O vs. O/H diagram and we discuss its large dispersion at all metallicity regimes. Using the same sample and a large grid of photoionization models covering very different values of the N/O ratio, we then study the most widely used strong-line calibrators of metallicity based on [NII] emission lines, such as N2 and O3N2. We demonstrate that these parameters underestimate the metallicity at low N/O ratios and viceversa. We investigate also the effect of the N/O ratio on different diagnostic diagrams used to discriminate narrow-line AGNs from star forming regions, such as the [OIII]/Hβ vs. [NII]/Hα, and we show that a large fraction of the galaxies catalogued as composite in this diagram can be, in fact, star forming galaxies with a high value of the N/O ratio. Finally, using strong-line methods sensitive to the N/O abundance ratio, like N2O2 and N2S2, we investigate the relation between this ratio and the stellar mass for the galaxies of the SDSS. We find, as in the case of the mass-metallicity relation, a correlation between these two quantities and a flattening of the relation for the most massive galaxies, which could be a consequence of the enhancement of the dispersion of N/O in the high metallicity regime.

Key words: ISM: abundances – HII regions: abundances – galaxies : starbursts, abundances

1 INTRODUCTION

The detection and measurement of emission lines in optical spectra are powerful tools for the derivation of the physical properties and the chemical status of star forming galaxies. In the star forming regions, the ionized gas absorbs the ultraviolet light coming from massive young stars and reemits it under the form of bright emission lines in the optical. However, the number of the detected emission lines and the quality of their measurement affect the methodology and the accuracy of the analysis of the properties of the host star forming regions. This is particularly true for the derivation of the metallicity. For instance, in the Giant Extragalactic HII Regions and in the Blue Compact Dwarf Galaxies, this analysis is based on the detection of the faint auroral lines, the so-called direct method, which allows to derive electron temperatures of the ionized gas and the chemical abundances using the intensities of the bright collisional forbidden emission lines.

This procedure is much more accurate when the determination of the thermal struture of the gas is based on the measurement of different electron temperatures, each one associated to different ionization regions (*e.g.* Garnett, 1992).

However, for the faint and distant galaxies and also for the metal-rich ones, the metallicity can only be derived using calibrators based on bright collisional emission lines. Many studies focused on the analysis of different calibrators of nebular metallicity based on strong lines (*e.g.* Pérez-Montero & Díaz, 2005; Kewley & Ellison, 2008). The calibration of these parameters can be empirical (*i.e.* using direct measurements of the oxygen abundance in the Local Universe) or theoretical (*i.e.* using photoionization models covering different physical properties). Unfortunately, the dispersion and the range of valid metallicity of each parameter depends strongly on the sample or on the input conditions of the models used to calibrate them.

Another issue, not well explored so far, appears with the strong-line methods aiming to derive the oxygen abun-

dance with emission lines of other elements (nitrogen, sulphur, etc). These calibrations can indeed depend on the relative abundance ratio of these elements. This is the case, for instance, for the S_{23} parameter (Díaz & Pérez-Montero, 2000; based on sulphur emission lines) which has been defined to compute oxygen abundances. This is also the case for some other calibrators based on [NII] emission lines, like the N2 parameter (among others Storchi-Bergmann et al., 1994; Van Zee et al., 1998 or Denicoló et al., 2002, hereafter DTT02) or the O3N2 parameter (Alloin et al., 1979; Pettini & Pagel, 2004, hereafter, PP04), which are used to derive the total abundance of oxygen.

There are some disagreements about the constancy of the ratio of different elements, even in the case when both have a primary origin, like oxygen and sulphur (*e.g.* Garnett, 2002.). In the case of the N/O ratio, which involves a primary element, oxygen, and another one with an extra secondary origin, like nitrogen, things are even more complicated. It is predicted that in the low metallicity regime most of the nitrogen has a primary origin, coming mainly from massive stars, while at higher metallicities the secondary production of nitrogen, coming mainly from low and intermediate mass stars, is dominant. Since the secondary production of nitrogen depends on the previous amount of oxygen stored in stars, via the CNO cycle, this implies a constant N/O ratio as a function of O/H at low metallicities (Edmunds & Pagel, 1978; Alloin et al., 1979) and a strong slope for higher metallicities.

However, numerous uncertainties remain regarding this scenario. First, the relative amount of primary nitrogen produced in massive stars (Chiappini et al., 2005) and in low- and intermediate-mass stars is not well known. This leads to an enhancement of the dispersion in both the low and the high metallicity regime. Second, the production of nitrogen depends sensibly on the stellar lifetimes and star formation efficiencies as derived from chemical evolution models, which increases also the dispersion in the predictions of these models (Mollá et al., 2006).

Our main aim with this work is to explore the observational dispersion of the N/O vs. O/H relation using a wide sample of HII regions and star-forming galaxies for which we derive consistently the oxygen and the nitrogen abundances using the direct method. We investigate also the effect of taking into account the real dispersion of this plot in the input conditions of photoionization models. We study the impact of the variation of the N/O ratio on different strong-line calibrators of nebular metallicity and on the diagnostic diagrams used to identify narrow line active galactic nuclei which are based on nitrogen emission lines. Finally, we apply our new calibrations based on N/O to study the behaviour of the N/O ratio as a function of the stellar mass in the galaxies of the local Universe. In the last section, we summarise our results.

2   DESCRIPTION OF THE SAMPLE

We compiled from the literature a sample of emission-line objects with available measurements of [OII], [OIII] and [NII] bright emission lines and, at least, one auroral emission line with high signal-to-noise ratio in order to estimate electron

Table 1. Bibliographic references for the emission line fluxes of the compiled sample

Reference	Object type[a]	Number
Bresolin et al., 2004	M51 GEHRs	10
Bresolin et al., 2005	GEHRs	31
Bresolin, 2007	M101 GEHRs	3
Garnett et al., 2004	M51 GEHRs	2
Guseva et al., 2003a	SBS 1129+576	2
Guseva et al., 2003b	HS 1442+650	2
Guseva et al., 2003c	SBS 1415+437	2
Hägele et al., 2006	HIIG	3
Hägele et al., 2008	HIIG	7
Izotov & Thuan, 1998	IZw18	2
Izotov et al. 1997	SBS 0335-018	1
Izotov et al., 1999	IZw18	1
Izotov et al., 2001	Tol 65	1
Izotov et al., 2004	HIIG	3
Izotov & Thuan, 2004	HIIG	33
Kehrig et al. 2004	HIIG	24
Kniazev et al.	SDSS galaxies	12
Lee et al., 2004	KISS galaxies	13
Melbourne et al., 2004	KISS galaxies	12
Pérez-Montero & Díaz, 2005	All	300
Van Zee, 2000	UGCA92	2
Vermeij et al., 2002	DRH	9
Total		475

[a] Name of the object or the sample or type of object in the sample: GEHR denotes Giant Extragalactic HII Regions; HIIG, HII Galaxies and DHR, Diffuse HII Regions.

temperatures and to derive ionic abundances using the direct method.

This compilation includes HII regions in our Galaxy and the Magellanic Clouds, Giant Extragalactic HII regions (GEHR), and HII Galaxies. Most of these objects belong to the compilation by Pérez-Montero & Díaz (2005) which was complemented with the sources listed in Table 1. The compilation contains 271 HII galaxies, 161 GEHRs and 43 HII regions of the Galaxy and the Magellanic Clouds, what gives a total of 475 objects.

3   PHOTOIONIZATION MODELS

A large grid of photoionization models was calculated to investigate the impact of the variation of the N/O abundance ratio on the estimation of several physical properties of HII regions, like electron temperatures, ionization correction factor (ICF) or empirical parameters based on [NII] emission lines.

We used the photoionization code Cloudy 06.02 (Ferland et al., 1998), taking as ionizing source the spectral energy distributions (SEDs) of O and B stars with the code

WM-Basic (version 2.11 [★], Pauldrach et al., 2001). The use of the SEDs of single stars allows to quantify the effective temperature of the models and does not affect strongly to the ionization structure of the gas as compared with SEDs from massive clusters. We assumed in all the models a radiation-bounded spherical geometry, a constant density of 100 particles per cm^2 and a standard fraction of dust grains in the interstellar medium. In all the models the calculation was stopped when the temperature was lower than 4000 K. We also assumed that the gas had the same metallicity than the ionizing stars, covering the values 0.05 Z$_\odot$, 0.2 Z$_\odot$, 0.4 Z$_\odot$, Z$_\odot$ and 2 Z$_\odot$, considering as the solar oxygen abundance the value measured by Allende-Prieto et al. (2001; 12+log(O/H) = 8.69). The other ionic abundances were set in solar proportions, except in the case of nitrogen, for which we considered values for all metallicities relative to oxygen of -0.50, -0.75, -1.0, -1.25, -1.50 and -1.75 in logarithmic units. Some depletion was taken into account for the chemical elements (C, O, Mg, Si and Fe) involved in the formation of dust grains. Regarding the other functional parameters we considered different values for the ionization parameter (log U = -3.5, -3.0, -2.5 and -2.0) and the effective temperature (T$_*$ = 40000 K, 45000 K and 50000 K). This produced a total of 360 photoionization models to cover the physical conditions of different ionized gas nebulae. Atomic data, including collision strengths in the models were consistent with those used in the calculation of chemical abundances in the compiled sample. They can be found in Table 6 of Hägele et al. (2008). We checked the influence of varying dielectronic recombination rate coefficients according with the most recent values (Badnell, 2006 and references therein), but we did not find any significant variation in our results.

4 RESULTS AND DISCUSSION

4.1 Physical conditions: electron density and temperature

All physical conditions were derived using the appropriate ratios of emission lines with the tasks TEMDEN, in the case of electron densities and temperatures, and IONIC, in the case of ionic abundances. These IRAF [†] tasks are based on the five-level statistical equilibrium model (De Robertis, Dufour & Hunt, 1987; Shaw & Dufour, 1995).

Following the procedure described in Pérez-Montero & Díaz (2003), we assigned the value of each derived electronic temperature to the calculation of the abundance of the corresponding ion. Electron densities were calculated for a subsample of 454 objects using the ratio of [SII] emission lines I(6717Å)/I(6731Å). We assumed a density of 100 particles per cm^2, typical in this kind of objects, in those objects without this ratio.

The electron temperature of O^{2+} was derived using the ratio of [OIII] emission lines (I(4959Å)+I(5007Å))/I(4363Å) for a subsample of 418 objects. For the objects that did not present the [OIII] auroral line, we derived t([OIII]) from the
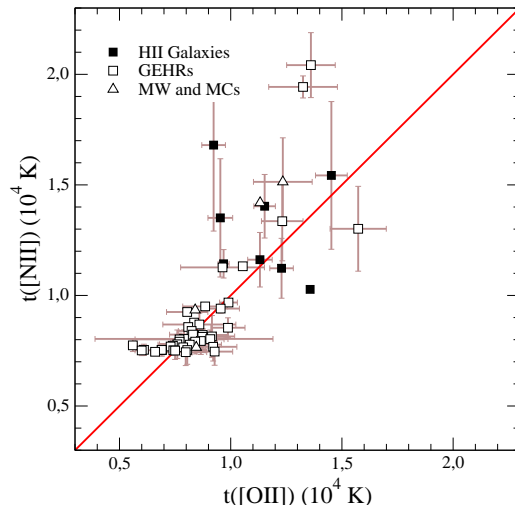
Figure 1. Relation between t([OII]) and t([NII]) for the sample of objects with a direct measurement of both temperatures. Black circles represent HII galaxies, white squares: Giant Extragalactic HII Regions, white triangles: HII regions in the Galaxy and the Magellanic Clouds. The solid red line represents the 1:1 relation.

available line temperatures of other ions: 33 from t([SIII]), using the empirical expression by Hägele et al. (2006), 20 from t([OII]), and 4 from t([NII])

The electron temperature of O$^+$ was derived using the [OII] emission line ratio (I(3727Å)/(I(7319Å)+I(7330Å)) for a subsample of 196 objects. The measurement of [OII] auroral lines presents higher uncertainties than in the case of [OIII] due to their lower signal-to-noise ratio and to a higher dependence on reddening correction, caused by their larger wavelength distance to the closest hydrogen recombination line. Besides, the [OII] auroral lines are contaminated by a small contribution of dielectronic recombination emission, although it does not contribute in quantities larger than the usual reported errors. Additionally, this ratio depends on electron density.

All these factors can enhance the uncertainty associated to the total chemical abundance of oxygen, especially in high metallicity - low excitation HII regions (Pérez-Montero & Díaz, 2005), but the estimation of O$^+$ using its corresponding measured electron temperature allows a better quantification of the associated errors in these objects.

For the objects with no direct estimation of t[OII], we used the relation between t([OII]) and t([OIII]) proposed by Pérez-Montero & Díaz (2003). This relation based on models has the following expression:

$$t([OII]) = \frac{1.2 + 0.002 \cdot n + \frac{4.2}{n}}{t([OIII])^{-1} + 0.08 + 0.003 \cdot n + \frac{2.5}{n}} \qquad (1)$$

and they take into account the dependence of t([OII]) on the electron density, n.

Regarding nitrogen, the electron temperature of N$^+$ can be derived from the emission-line ratio (I(6584Å)+I(6548Å))/I(5755Å) in very few objects, due to the intrinsic weakness of the corresponding auroral line. We derived this temperature for a subsample of 88 objects. In Figure 1, we show the relation between t([OII]) and t([NII]) for those objects of the sample with a direct determination of both temperatures. As we see, the assumption of a unique
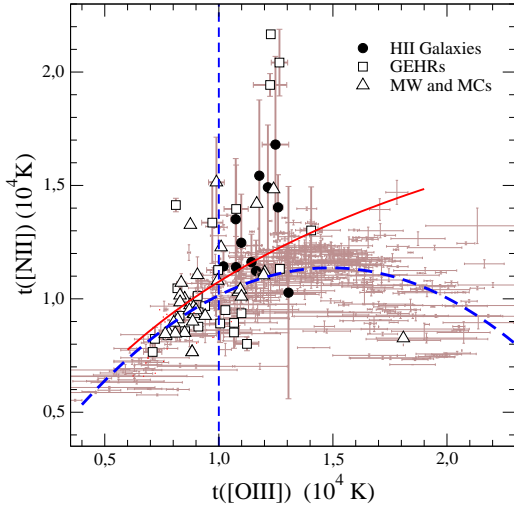
Figure 2. Relation between t([OIII]) and t([NII]) for the sample of objects with a direct measurement of both temperatures. Symbols are the same as in the previous figure. The solid red line represents the best quadratic fit to the photoionization models. The brown error bars represent the values of t([NII]) derived from the relation of Thurston et al. (1996) and the dashed blue line its best quadratic fit. Vertical dashed line shows the upper limit (10000 K) of validity originally defined for the Thurston et al. relation.

low-excitation electron temperature is well justified for the most part of the objects. Nevertheless, the dispersion in this diagram and the deviation between these temperatures in objects with thermal structures affected by the geometry of the gas lead us to take independent estimations of these temperatures in all cases.

Therefore, for those objects without a direct estimation of t([NII]), we derived an independent relation between this temperature and t([OIII]) based on the grid of photoionization models described in Section 3. The obtained relation is well described by the following quadratic fit:

$$t([NII]) = \frac{1.85}{t([OIII])^{-1} + 0.72} \quad (2)$$

This relation does not depend on the assumed N/O ratio in the range of temperatures covered by the models (from 6000 to 18000 K). We show it in Figure 2 together with the objects with a direct determination of both t([OIII]) and t([NII]). As we can see, the relation deduced from the models overestimates t([NII]) at very low temperatures as compared with the direct measurements. However, in the range of T([OIII]) between 7000 and 14000 K, the relation covers correctly the sample, with the exception of some objects with very high values of t([NII]). This could be due to different problems in the measurement of the weak auroral line of [NII]. In these cases, we took the temperature predicted by the models to calculate nitrogen abundances.

We show in the same Figure 2 the temperatures of [NII] based on the relation proposed by Thurston et al. (1996), based also on models, for the high metallicity range (Z> $0.3Z_\odot$)

$$t([NII]) = 0.6065 + 0.1600x + 0.1878x^2 + 0.2803x^3 \quad (3)$$

where x is based on the intensities of the emission lines of [OII] and [OIII]

$$x = \log R_{23} = \log \left(\frac{I([OII]3727 + [OIII]4959, 5007)}{I(H\beta)} \right) \quad (4)$$

The values of t([NII]) deduced from this relation are plotted in Figure 2 with the best quadratical fit. This relation is almost identical to ours for low excitation conditions (T<10000 K), which is the range of validity originally proposed. The two relations diverge for higher temperatures, leading to non-negligible deviations in the calculation of the ionic abundances if it is not used properly.

4.2   Ionic and total chemical abundances

The ionic abundances were calculated using the most prominent emission lines of each ion and the appropriate electron temperature. To calculate O^+ ionic abundances, we used the intensity of the [OII] line at 3727 Å, except in the case of 11 of the 12 very low metallicity HII Galaxies identified by Kniazev et al. (2003) in the SDSS catalogue without any measurement of the [OII]λ3727 line. For these objects the O^+ abundance was derived using the emission lines of [OII] at 7319 Å and 7330 Å. The derivation of O^{2+} abundances was based on the [OIII] emission lines at 4959 Å and 5007 Å. The O^+ and O^{2+} abundances were then used to calculate the total abundance of oxygen relative to hydrogen using the following assumption:

$$\frac{O}{H} \simeq \frac{O^+ + O^{2+}}{H^+} \quad (5)$$

Abundances of N^+ were calculated using the [NII] emission lines at 6548 Å and 6584 Å Then it is possible to derive the total nitrogen abundance and the N/O ratio taking the following approximation:

$$\frac{N}{O} \simeq \frac{N^+}{O^+} \quad (6)$$

based on the similarity of the ionization structures of both N and O. This leads to the following assumption about the ICF of N^+:

$$ICF(N^+) \simeq \frac{O}{O^+} \simeq \frac{O^+ + O^{2+}}{O^+} \quad (7)$$

which is in good agreement with our models.

4.3   Behaviour of N/O with metallicity

We show in Figure 3 the relation between the N/O ratio and the oxygen abundance for the sample of HII regions and star-forming galaxies whose oxygen and nitrogen abundances were calculated consistently following the direct method (see Section 2).

We also show the prediction from closed-box chemical evolution models concerning the production of secondary nitrogen (yields from Henry et al., 2000), in the high metallicity regime, and the contribution of an extra amount of primary nitrogen at lower metallicities.

As we can see, although these predictions are followed in average, the observations show a very high dispersion, especially at high metallicities. This dispersion is real and does not depend on the methodology we have used to derive abundances. For instance, the assumption of a single electron temperature for the calculation of N^+ and O^+ only reduces the standard deviation in the distribution of N/O
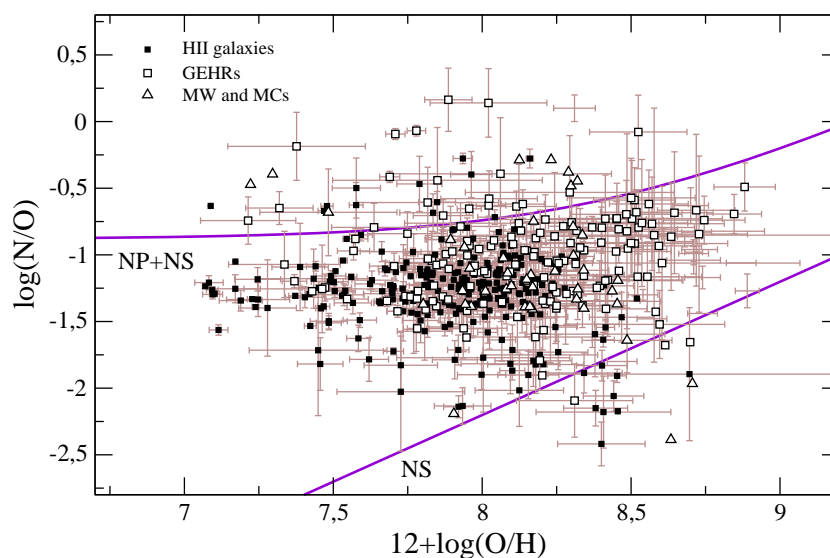
Figure 3. Relation between metallicity, represented by the abundance of oxygen, and the N/O ratio for different objects: the sample of HII regions whose abundances were calculated using the direct method in this paper are represented by the same symbols as in Figure 1. Solid line represents the prediction of chemical evolution closed-box models of primary and secondary nitrogen at all ranges of metallicity. These models were calculated taking the yields from Henry et al. (2000)

in 0.05 dex. At low metallicities, the dispersion is lower because nitrogen has essentially a primary origin, produced mainly by massive stars and with no dependence on the previous amount of oxygen stored in stars. However, even in this regime, there are some objects which exceed the relative amount of nitrogen predicted by the models. This is the case of some HII galaxies and GEHRs, with a probable extra production of primary nitrogen. Between the causes of the uncertainty in the prediction of primary N, it is the rotation velocity of stars and the amount of metals loss in winds, as in Wolf-Rayet stars (Meynet & Maeder, 2005).

For high metallicities the dispersion increases as a consequence of both primary and secondary production of nitrogen in the same metallicity regime. It is known that some intermediate-mass stars can produce an extra amount of primary nitrogen (*e.g.* Renzini & Voli, 1981). We also find some HII galaxies with extremely low values of N/O. This type of objects was already described in some works in which they are often associated with UV-bright galaxies (*e.g.* Contini et al., 2002; Mallery et al., 2007). For the same metallicity, some HII regions in spirals show very high values of the N/O ratio but, in this case, Bresolin et al. (2005) claim that the N abundances determined from the [NII] auroral line are not very reliable.

The simultaneous analysis of all these objects in the same diagram leads to the conclusion that in the same metallicity bin, we can find variations in the N/O ratio of more than one order of magnitude and implies the impossibility of finding an unique model that predicts the behaviour of this ratio for all the metallicity regimes.

4.4 Metallicity strong-line methods based on [NII]

In this section, we investigate the effect of the N/O abundance ratio on two metallicity empirical calibrators based on [NII] emission lines, namely N2 and O3N2.
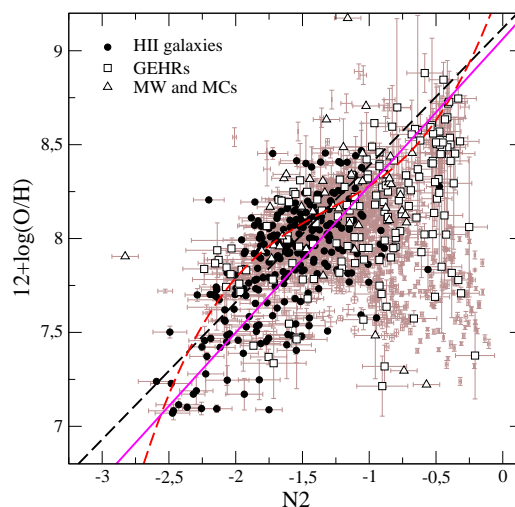

Figure 4. Relation between the N2 parameter and the oxygen abundance for the studied objects. Symbols stand for the same types of objects as described in previous figures. Black dashed line represents the DTT02 calibration, red dashed line the PP04 calibration and magenta solid line the linear fit to the data.
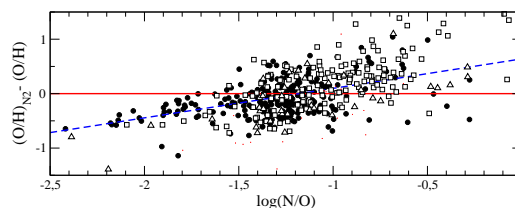

Figure 6. Residuals between the oxygen abundances derived from the N2 empirical calibration and the abundances derived using the direct method as a function of the N/O ratio. The solid line represents the residual zero and the dashed line the linear fit of the points.
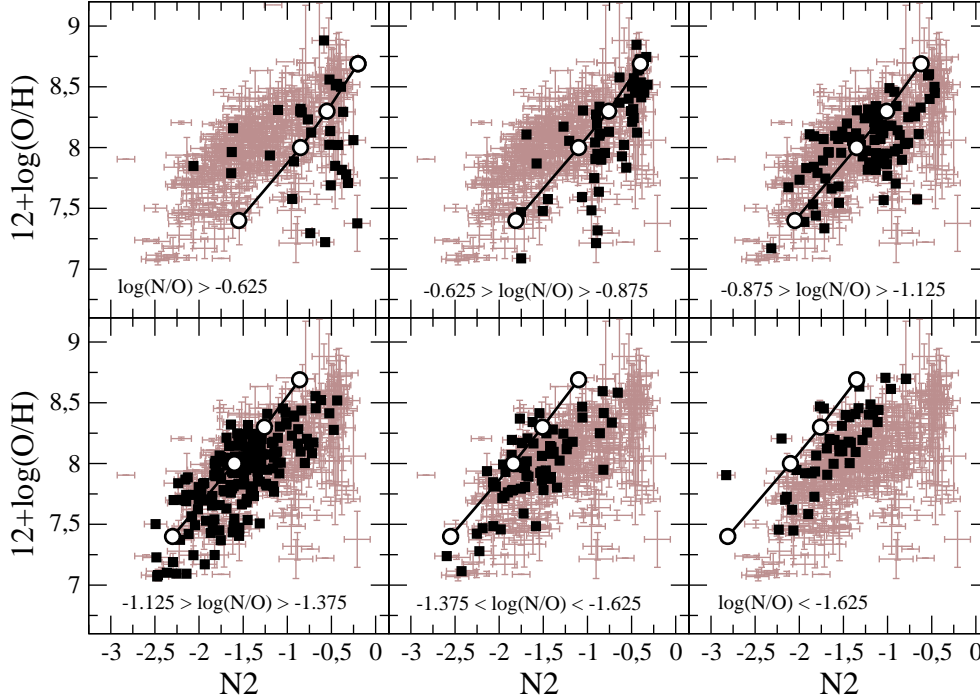
Figure 5. Relation between oxygen abundance and the N2 parameter for different values of the N/O ratio. All the sample is shown in each plot but only those objects with the corresponding N/O value are marked as black squares. We show too as white circles the photionization models corresponding to these values of N/O: -1.75, -1.50, -1.25, -1.00, -0.75 and -0.50 from right to left and from bottom to top, respectively.

4.4.1 The N2 parameter

The N2 parameter, defined as:

$$N2 = log\left(\frac{I([N_{II}]6584\text{Å})}{I(H\alpha)}\right) \qquad (8)$$

has been extensively used in the literature to derive oxygen abundances. (*e.g.* Storchi-Bergmann et al., 1994, Van Zee et al., 1998, DTT02). In particular, DTT02 proposed the following linear relation:

$$12 + log(O/H) = 9.12 + 0.73 \cdot N2, \qquad (9)$$

based on a sample of HII regions with metallicities derived in the low metallicity regime using the direct method and using other strong-line methods in the high metallicity regime. Another extensively used calibration of this parameter is this polynomical fit proposed by PP04.

$$12 + log(O/H) = 9.37 + 2.03 \cdot N2 + 1.26 \cdot N2^2 + 0.32 \cdot N2^3 \quad (10)$$

The used sample in this case is composed of HII regions whose oxygen abundance were mostly derived using the direct method, except in the case of some oversolar metallicity objects, whose metallicities were derived from photoionization models.

The main advantage of this parameter lies in its complete independence on reddening correction or flux calibration, due to the close wavelength of the involved emission lines and, contrary to the R_{23} parameter, in its single-valued relation with metallicity up to solar values. In Figure 4, we show the relation between the N2 parameter and the oxygen abundance for our sample of objects, along with the calibrations of DTT02 and PP04. The least-squares bisector linear

fit (Isobe et al., 1990) of the points is plotted in Figure 4 and it gives the following expression:

$$12 + log(O/H) = 0.79 \cdot N2 + 9.07 \qquad (11)$$

However, this fit does not provide a lower dispersion as compared to the previous calibrations: the standard deviations of the residuals is 0.34 dex, while it is 0.33 in the case of the DTT02 calibration and 0.32 dex for PP04. The origins of this dispersion are studied in Pérez-Montero & Díaz (2005), who concluded that higher ionization parameters and effective temperatures lead to higher metallicities as derived from N2. Additionally, a substantial part of the observed dispersion is due to N/O variations, as a consequence of using nitrogen emission lines to derive oxygen abundances.

In Figure 5, we show the studied sample divided in bins of log(N/O), and compared with sequences of photoionization models with the same values of N/O. These sequences of models have as input conditions the values of T_* and log U most plausible for each metallicity (high T_* and log U for low metallicity and viceversa), but they have not been used to recalibrate the parameter and they are only used to check how the N2 parameter varies as a function of N/O in the models.

As we can see, it exists a strong correlation between the metallicity derived from the N2 parameter and the N/O ratio in such a way that the metallicity predicted by N2 is overestimated in those objects with a high N/O ratio and vice-versa. This trend is confirmed when we compare models and the observations, although the dispersion in the observations is higher for high values of N/O. Regarding models, no consistent values were found for oversolar abundances
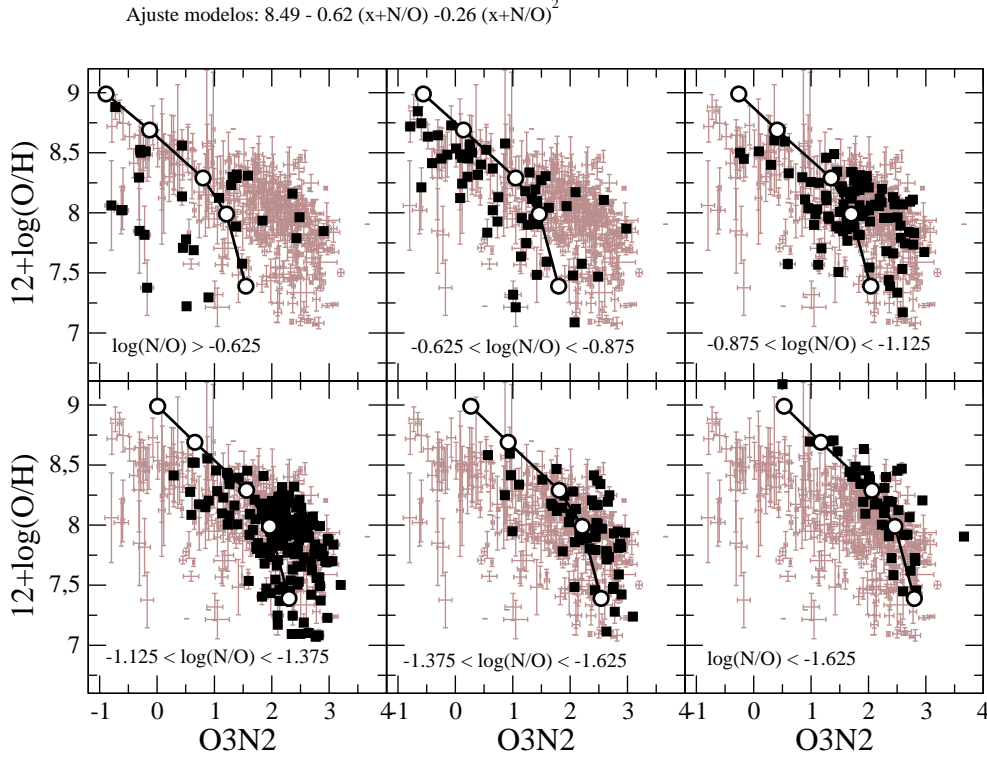
Ajuste modelos: 8.49 - 0.62 (x+N/O) -0.26 (x+N/O)^2

Figure 8. Relation between oxygen abundance and the O3N2 parameter for different values of the N/O ratio. The full sample is shown in each plot but only those objects with the corresponding N/O value are marked as black squares. We show also as white circles the photionization models corresponding to these values of N/O: -1.75, -1.50, -1.25, -1.00, -0.75 and -0.50 from right to left and from bottom to top.
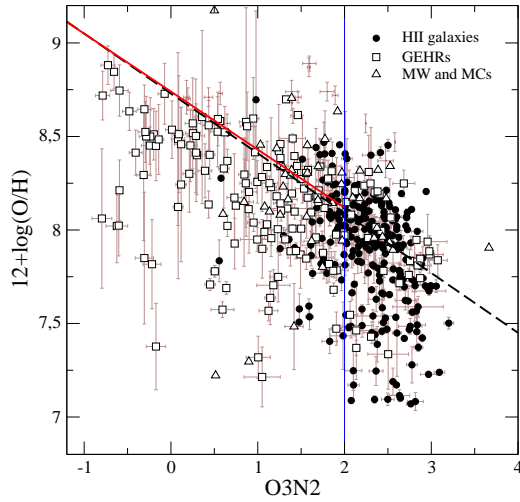
Figure 7. Relation between the O3N2 parameter and the oxygen abundance for the studied objects. Symbols stand for the same types of objects as described in previous figures. Black dashed line represents the PP04 calibration and blue vertical solid line shows the limit of validity of this calibration (O3N2 < 2)

because the N2 parameter saturates in this high metallicity regime.

We quantified the dependence of the calibration of the N2 parameter on the N/O ratio. To do so, we analysed the residuals between the metallicities derived from N2 and from the direct method as a function of N/O. This is shown in

Figure 6 with its best linear fit, which gives the following result:

$$\Delta(O/H) = 0.56 \cdot \log(N/O) + 0.66 \qquad (12)$$

Taking into account this correction, we can adopt the following expression for the relation between N2 and the oxygen abundance:

$$12 + \log(O/H) = 0.79 \cdot N2 - 0.56 \cdot \log(N/O) + 8.41 \qquad (13)$$

which reduces the dispersion of the metallicity derived using N2 to 0.21 dex.

4.4.2 The O3N2 parameter

The O3N2 parameter is defined as:

$$O3N2 = \log \left(\frac{I([O\text{III}]5007\text{Å})}{I(H\beta)} \times \frac{I(H\alpha)}{I([N\text{II}]6584\text{Å})} \right) \qquad (14)$$

and was used as an estimator of metallicity by Alloin et al. (1979), although the most widely used calibration is a linear fit proposed by PP04:

$$12 + log(O/H) = 8.73 - 0.32 \cdot O3N2 \qquad (15)$$

We show in Figure 7 the relation between the O3N2 parameter and the oxygen abundances for our sample. Contrary to N2, the relation is not clearly linear. For the low metallicity regime (O3N2 > 2) this parameter does not correlate with the metallicity. This means that for HII galaxies, which populate the low metallicity regime, objects with
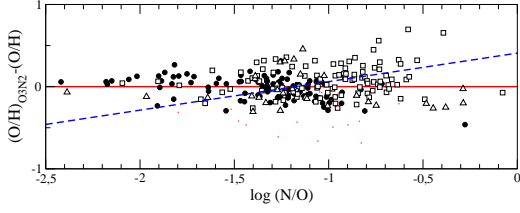
Figure 9. Residuals between the oxygen abundances derived from the O3N2 empirical calibration and the abundances derived using the direct method as a function of the N/O ratio. The solid line represents the residual zero and the dashed line the linear fit of the points.

a difference of an order of magnitude in metallicity have very similar values of O3N2. However, in the high metallicity regime (O3N2 < 2), we can perform a least-square bisector linear fit to our data, which gives:

$$12 + log(O/H) = 8.74 - 0.31 \cdot O3N2 \qquad (16)$$

and which is almost identical to the relation proposed by PP04. Both relations present a standard deviation of the residuals of 0.32 dex.

For the O3N2 parameter we show in Figure 8 the same data but divided in bins corresponding to different N/O ratios. The models corresponding to different values of log(N/O) (-1.75, -1.50, -1.25, -1.00, -0.75 and -0.50) are shown too. Despite of the large dispersion found for high values of N/O, as in the case of N2, we see a strong dependence of the relation on the N/O ratio for both the models and the observations. This implies that the metallicity predicted by O3N2 is overestimated in those objects with a high value of the N/O ratio.

The linear relation existing between the O3N2 parameter and the oxygen abundance is valid only for 12+log(O/H) > 8 but, contrary to N2 parameter, it can be used up to very high metallicities, larger than twice the solar value, according to the models.

We show in Figure 9, the residuals between the metallicities derived from O3N2 and the abundances obtained following the direct method in the high metallicity regime (12+log(O/H) > 8) as a function of the N/O ratio. The least-square bisector linear fit to the data points has the following expression:

$$\Delta(O/H) = 0.35 \cdot \log(N/O) + 0.41 \qquad (17)$$

The use of this correction to the linear fit of O3N2 at high metallicities reduces the dispersion to 0.23 dex, using the following expression:

$$12 + \log(O/H) = 8.33 - 0.31 \cdot O3N2 - 0.35 \cdot \log(N/O) \ (18)$$

4.5 Strong-line methods to derive the N/O ratio

The N2O2 parameter defined as:

$$N2O2 = \log \left(\frac{I([N\textsc{ii}]6584\text{Å})}{I([O\textsc{ii}]3727\text{Å})} \right) \qquad (19)$$

has been proposed as an estimator of oxygen abundance by Kewley & Dopita (2002). In the left panel of Figure 10 we show the relation between this parameter and the oxygen abundance for our sample. As it was already stated

by Kewley & Dopita (2002), this parameter is sensitive to the metallicity in the high metallicity regime only, while for low metallicity objects, the parameter is almost constant. In fact, the relation between N2O2 and metallicity resembles the relation between N/O and O/H because it reproduces the ratio between the abundances of oxygen and nitrogen: a constant value of the nitrogen abundance in the low metallicity regime and a strong variation as a function of metallicity for high metallicities.

In the right panel of Figure 10 we show the relation between N2O2 and the N/O ratio. In this case, we find a linear correlation for all metallicity regimes, with the exception of some HII galaxies with very low values of N/O. The least-squares bisector linear fit between this parameter and the N/O ratio gives

$$\log(N/O) = 0.93 \cdot N2O2 - 0.20 \qquad (20)$$

with a standard deviation of the residuals of 0.24 dex. This relation is slightly shallower than the linear fit proposed by Pérez-Montero & Díaz (2005) for a sample of HII galaxies. Therefore, the ratio between [N\textsc{ii}] and [O\textsc{ii}] lines constitutes a powerful tool to derive N/O ratio. Moreover it allows the correction of the metallicity estimated from the N2 parameter or, in the case of the oversolar metallicity regime, from the O3N2 parameter.

Another calibrator based on [N\textsc{ii}] is the S2N2 parameter. Originally introduced by Sabbadin et al. (1977) it has been proposed to derive metallicities by Viironen et al. (2007). To keep the consistency with previous described parameters, we define this calibrator as follows:

$$N2S2 = \log \left(\frac{I([N\textsc{ii}]6584\text{Å})}{I([S\textsc{ii}]6717, 6731\text{Å})} \right) \qquad (21)$$

In the left panel of Figure 11, we show the relation between this parameter and the abundance of oxygen in our sample. We find again the same trend observed in the case of N2O2: a constant value of the parameter for low metallicities and a variation for high metallicities. This is a consequence of using a ratio of emission lines coming from sulphur, which is an α element whose origin is primary, as in the case of oxygen, and nitrogen, whose origin can be primary or secondary. As for N2O2 we explored the correlation between this parameter and the N/O ratio, which is shown in right panel of Figure 11. This relation is again linear with the exception of some HII galaxies with very low values of N/O. The least-squares bisector linear fit of this parameter as a function of the N/O ratio gives:

$$\log(N/O) = 1.26 \cdot N2S2 - 0.86 \qquad (22)$$

with a standard deviation of the residuals of 0.31 dex, a slightly higher dispersion than in the case of N2O2 caused probably by the variations in the S/O ratio, taking into account that uncertainties due to reddening and flux calibrations are lower than in the case of N2O2. Nevertheless, N2S2 is more suitable to estimate the N/O ratio than N2O2 due to the simultaneous measurement of all the involved lines in many observations.

4.6 Spectral classifications based on [N\textsc{ii}] lines

Diagnostics based on [N\textsc{ii}] emission lines are commonly used to classify emission-line galaxies according to their domi-
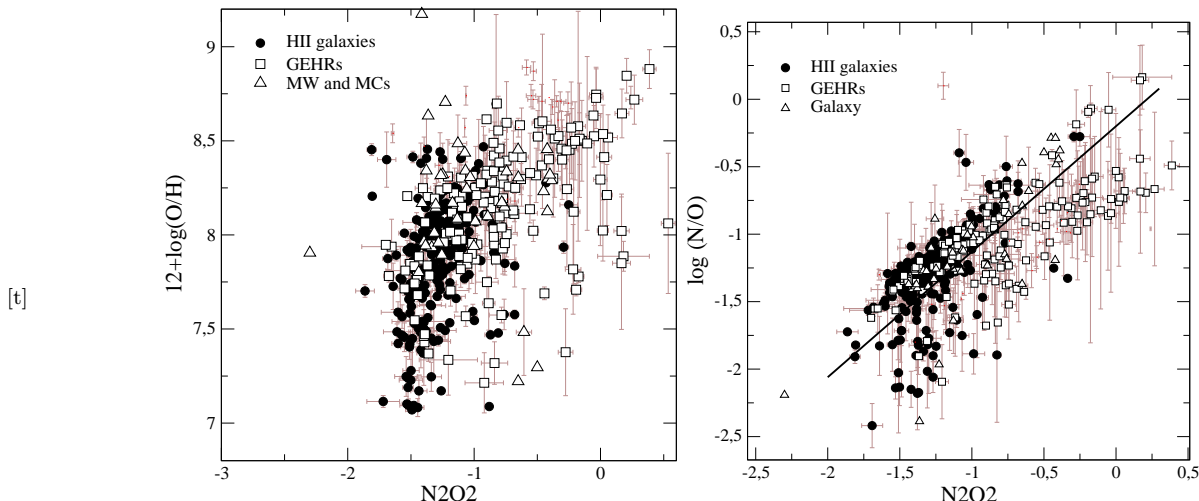
Figure 10. Relation between the N2O2 parameter and the oxygen abundance (left panel) or the N/O abundance ratio (right panel) for the objects described in Section 2. The solid line represents the best linear fit to the sample.
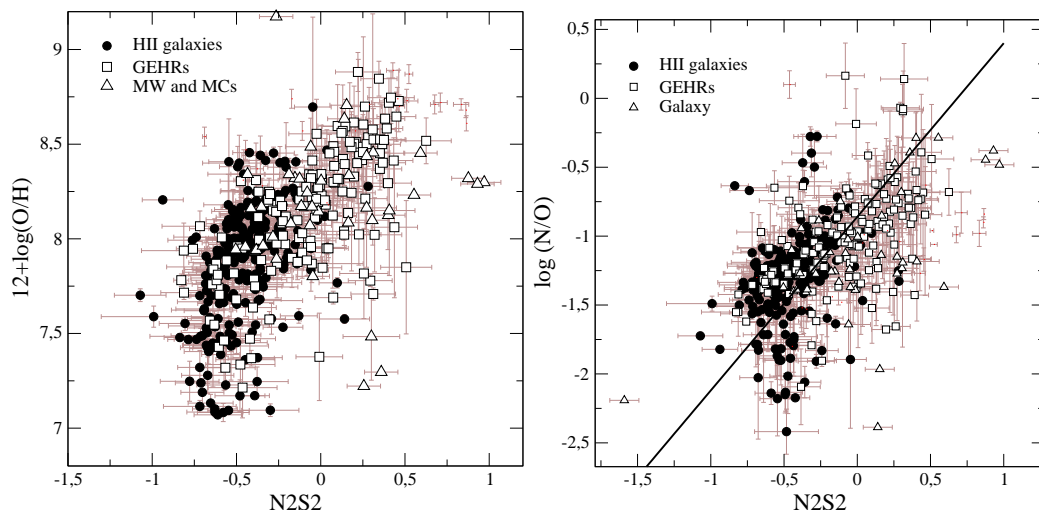

Figure 11. Relation between the N2S2 parameter and the oxygen abundance (left panel) or the N/O abundance ratio (right panel) for the objects described in Section 2. The solid line represents the best linear fit to the sample.

nant mechanism of ionization. In particular, it is possible to distinguish between ionization due to the UV radiation coming from massive young stars (star-forming regions) or from an active galactic nucleus (hereafter AGN). Among these diagnostics, the first diagrams proposed by Baldwin, Philips & Terlevich (1981), also known as BPT diagrams, are based on four emission-line ratios, namely [OIII]/Hβ, [NII]/Hα, [SII]/Hα and [OI]/Hα. Due to the impossibility of detecting at the same time these emission lines in most of the deep surveys of high-redshift galaxies based on optical spectroscopy (eg. VVDS, zCOSMOS), because of their limited spectral range, some other diagnostic diagrams were proposed to overcome this issue. This is the case of the blue diagnostic diagram, proposed by Lamareille et al. (2004), which involves the [OIII] and [OII] lines or the red diagnostic, which relates empirically the [NII]/Hα and [SII]/Hα ratios.

Generally in these diagnostic diagrams, the regions of star-forming galaxies and narrow-line AGNs (Seyfert 2 and LINERs) are separated using photoionization models

(e.g. Kewley et al. 2001), or empirically (Kauffmann et al., 2003). In Figure 12 we show the diagnostic diagrams mentionned above using the emission-line galaxies listed in the MPA/JHU Data catalogue of the Sloan Digital Sky Survey[‡] DR7 release. We have kept only the galaxies with a signal-to-noise ratio of at least 5 in all the involved lines. This excludes all the objects at redshift z<0.02, whose [OII] 3727 Å emission line is not observed in the SDSS catalogue and giving as a result a total of 101753 emission line galaxies.

We corrected for reddening the emission-line intensities using the Balmer decrement. In the diagram [OIII]/Hβ vs. [NII]/Hα, the separation curves proposed by Kewley et al. (2001) and Kauffmann et al. (2003) do not coincide. In fact, as it is described in Kewley et al. (2006), the number of star-forming galaxies predicted by the empirical separation is overestimated when compared with the theoretical rela-
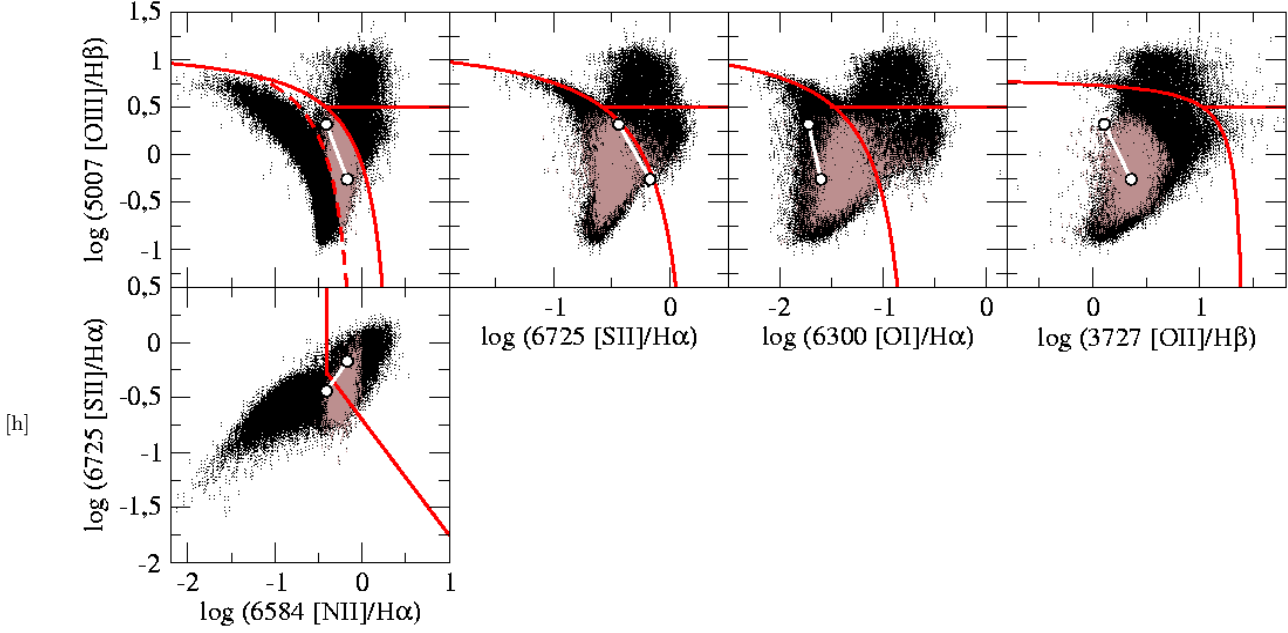
[‡] Available at http://www.mpa-garching.mpg.de/SDSS/

Figure 12. Different diagnostic diagrams used to separate star forming galaxies and narrow-line AGNs. We show in the four top panels the relations between [OIII]/Hβ and from left to right: [NII]/Hα, [SII]/Hα, [OI]/Hα and [OII]/Hβ. The bottom panel represents the relation between [NII]/Hα and [SII]/Hα. Brown points represent *composite* galaxies (see text) whose log(N/O) as derived from the N2O2 parameter is higher than -0.5. Solid lines represent the curves proposed by Kewley et al. (2003) to separate star forming galaxies (bottom left) and AGNs (top right) stay. The dashed line in the first panel represents the empirical curve predicted by Kauffmann et al. (2003). Finally, the white points represent two different models of star forming regions with high metallicity (Z=0.02Z$_\odot$) and high N/O ratio (−0.5).

tion. This is explained in terms of a population of *composite* objects, whose ionization is due partially to the star formation and to the presence of an active nucleus. This agrees with the fact that [NII] emission lines are more sensitive to the presence of X-ray sources and, therefore, they allow to probe the presence of low-activity active nuclei in some galaxies classified as star-forming.

Nevertheless, the enhancement of the N/O abundance ratio due to peculiar chemical histories can lead to high values of the [NII] emission lines in some star-forming galaxies. In all panels of Figure 12 we identify those SDSS galaxies catalogued as *composite* following Kewley's criterion and whose log(N/O) is higher than −0.5 as derived using the N2O2 parameter. This represents a 53% of all the *composite* galaxies. At same time, most of these *composite*-high N/O galaxies lie in the bottom and left-hand side of the Kewley et al. (2003) classification of the other diagrams: 86% in the [SII]/Hα diagram, 76% in the [OI]/Hα and 99.8% using [OI]/Hβ. This indicates that a fraction of the galaxies classified as *composite* in the NII]/Hα vs. [OIII]/Hβ diagram could correspond to star-forming galaxies with high values of the N/O ratio.

This conclusion is partially supported by some of the results coming from photoionization models. In Figure 12 we show also the position of two of the models described in Section 3. In this case, these models have an ionization coming from a WM-Basic star with T$_*$=45000 K, an ionization parameter of respectively log U = −2.5 and −3.0, a solar metallicity and a log(N/O) = −0.5. These models, which appear in the *composite* region in the diagram NII]/Hα vs.[OIII]/Hβ, are located below and in the left-hand side of

the Kewley et al. (2003) classification in the rest of the BPT diagrams, and in the blue diagnostic diagram too. Only in the red diagnostic diagram between [NII]/Hα and [SII]/Hα, the model with a lower ionization parameter lies in the AGN region. We did not find that the number of AGNs predicted by this red diagnostic diagram is higher than in the others not depending on [NII] lines, but it is possible that the AGN region was contaminated with some star-forming objects with high N/O.

4.7 The relation between the N/O abundance ratio and the stellar mass

As an application of the strong-line methods based on [NII] emission lines to derive N/O, we studied the relation between this abundance ratio and the stellar mass of the star-forming galaxies selected in the DR7 of the SDSS. The stellar masses taken from the DR7 SDSS catalogue were derived from their SED fitting (Kauffmann et al., 2003). As before, we kept only those galaxies whose [OII], Hα, [NII] and [SII] emission-line fluxes had S/N better than 5. This excludes as well the galaxies with redshift lower than 0.02, with no measurement of the [OII] emission line. We also excluded narrow-line AGNs as identified in the [OIII]/Hβ vs. [NII]/Hα diagnostic diagram, according to the Kauffman et al. (2003) curve and, therefore, we take all the *composite* galaxies.

The relation between N/O and stellar masses for SDSS galaxies is shown in Figure 13. In the left panel, the N/O ratios were derived using the N2O2 parameter, while in the right panel they were obtained from N2S2. The N/O values in this last case are, in average, 0.25 dex lower. This differ-
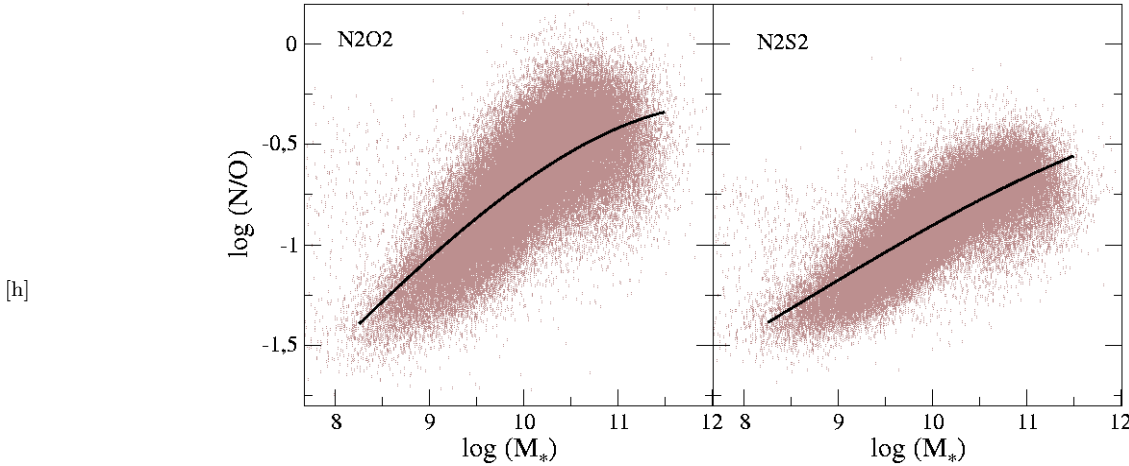
Figure 13. Relation between stellar mass and the N/O ratio for the star forming galaxies of the SDSS DR7 catalogue. In the left panel N/O ratios have been derived using the N2O2 parameter and in right panel, from N2S2. The solid lines in both panels represent the polynomial fit of 3th order to the sample.

ence is much higher than the expected associated error to the lines, to the calibrations or to the reddening, so it is possible that [OII] emission lines were underestimated in these objects due to their proximity to the instrumental edge in SDSS observations. However, we observe in both panels a global trend for a higher N/O ratio at higher stellar masses. This could be a consequence of the fact that the most massive galaxies have evolved more quickly and, hence, they have in average higher metallicities and higher N/O ratios. We also observe a flattening of the relation for the most massive galaxies. This is caused mainly by the same flattening observed in the mass-metallicity relation (Tremonti et al., 2004), but it can be related to the high dispersion in the N/O vs. O/H diagram at high metallicities, where the relative production of primary and secondary nitrogen is quite uncertain. Although the variation in the N/O ratio can be higher than an order of magnitude for each mass bin, we provide the cubic polymial fits to the data in both diagrams to be used as a reference of the local Universe. In the case of the N/O ratio obtained using N2O2, we obtain the following relation:

$$y = -1.884 - 0.846 \cdot x + 0.172 \cdot x^2 - 0.0075 \cdot x^3 \qquad (23)$$

and for N/O ratios obtained from the N2S2 parameter:

$$y = -1.5793 - 0.467 \cdot x + 0.088 \cdot x^2 - 0.0034 \cdot x^3 \qquad (24)$$

where y is log(N/O) and x is log(M$_*$), in solar units.

5 SUMMARY AND CONCLUSIONS

In this work we investigated the impact of the N/O ratio on some strong-line methods commonly used to derive the metallicity of star-forming galaxies, and on different diagnostic diagrams based on [NII] emission lines.

To this aim, we compiled a sample of ionized gaseous nebulae with available measurements of the [OII], [OIII] and [NII] strong lines and, at least, one auroral line. This allowed us to derive electron temperatures and ionic abundances following the direct method. The collected sample corresponds to very different metallicities and ionization conditions. We

also calculated a large grid of photoionization models covering these many different conditions, including a range in log(N/O) between -1.75 and -0.50. As expected, we did not find any significant dependence on N/O, both for the ICF(N$^+$) and for the relation between t([OIII]) and t([NII]). The inner thermal structure of the ionized gas is controlled mainly by the total metal content of the nebula and the relative abundances of different elements has a negligible impact on it.

The study of the relation between the N/O abundance ratio and the metallicity for the same sample confirmed a very high dispersion for both the low and high metallicity regimes, due to the uncertainties in the relative production of primary and secondary nitrogen at all metallicity regimes. We also studied the dependence of the widely used strong-line methods N2 and O3N2 on the N/O ratio. Both observations and models confirm that these two parameters underestimate the oxygen abundance for objects with low N/O ratios and viceversa. Taking into account the value of the N/O ratio in the calibrations can reduce 0.10 dex the dispersion of the residuals. However, this dispersion cannot be reduced further due to the intrinsic heterogeneity in the considered sample.

The strong-line calibrators which depend on ratios between the [NII] emission line and another low-excitation line, like [OII] or [SII] (namely N2O2 and N2S2) can be used to derive the N/O ratio at all ranges of metallicity.

We explored the impact of the N/O ratio on the diagnostic diagram [OIII]/Hβ vs. [NII]/Hα. We showed that the region of this diagram defined by Kewley et al. (2006) for composite galaxies can also be populated by star-forming galaxies with a high N/O ratio. More work in this issue must be done to quantify the contribution of both populations to this part of the diagram.

Finally, by using the strong-line methods to derive N/O, we studied the variation of this abundance ratio with the stellar mass of the SDSS galaxies. Despite the non-negligible offset between the ratios obtained using N2O2 and N2S2, both diagrams are consistent when predicting a enhancement of the average N/O for the most massive galaxies, consequence of a more evolved status of these galaxies. This

correlation is flatter for the most massive galaxies, which could be consequence of the same flattening observed in the mass-metallicity relation and of a higher dispersion of the N/O ratio for higher metallicities.

REFERENCES

Allende Prieto, C., Lambert, D. L., & Asplund, M. 2001, ApJL, 556, L63

Alloin, D., Collin-Souffrin, S., Joly, M., Vigroux, L., 1979, A&A, 78, 200

Badnell N. R., 2006, A&A, 447, 389

Baldwin J. A., Phillips M. M., Terlevich R., 1981, PASP, 93, 5

Bresolin, F. 2007, ApJ, 637, 751

Bresolin, F., Garnett, D. R., & Kennicutt, R. C., Jr. 2004, ApJ, 615, 228

Bresolin F., Schaerer D., González Delgado R. M., Stasińska G., 2005, A&A, 441, 981

Chiappini, C., Mateucci, F., & Ballero, K., 2005, A&A, 437, 429

Contini, T., Treyer, M.A., Sullivan, M., Ellis, R.S. 2002, MNRAS, 330, 75

De Robertis, M.M., Dufour, R.J. & Hunt, R.W. 1987, JRASC, 81, 195

Denicoló G., Terlevich R., Terlevich E., 2002, MNRAS, 330, 69 (DTT02)

Díaz A. I., Pérez-Montero E., 2000, MNRAS, 312, 130

Edmund, M.G., Pagel, B.E.J. 1978, MNRAS, 185, 77P

Erb, D. K., Steidel, C. C., Shapley, A. E., Pettini, M., Reddy, N. A., & Adelberger, K. L. 2006, ApJ, 646, 107

Ferland, G. J. Korista, K.T. Verner, D.A. Ferguson, J.W. Kingdon, J.B. Verner, & E.M. 1998, PASP, 110, 761

Garnett D. R., 1992, AJ, 103, 1330

Garnett, D. R. 2002, ArXiv Astrophysics e-prints, arXiv:astro-ph/0211148

Garnett D. R., Kennicutt R. C., Jr., Bresolin F., 2004, ApJ, 607, L21

Guseva, N. G., Papaderos, P., Izotov, Y. I., Green, R. F., Fricke, K. J., Thuan, T. X., & Noeske, K. G. 2003a, A&A, 407, 75

Guseva, N. G., Papaderos, P., Izotov, Y. I., Green, R. F., Fricke, K. J., Thuan, T. X., & Noeske, K. G. 2003b, A&A, 407, 91

Guseva, N. G., Papaderos, P., Izotov, Y. I., Green, R. F., Fricke, K. J., Thuan, T. X., & Noeske, K. G. 2003c, A&A, 407, 105

Hägele G. F., Díaz Á. I., Terlevich E., Terlevich R., Pérez-Montero E., Cardaci M. V., 2008, MNRAS, 383, 209

Hägele, G. F., Pérez-Montero, E., Díaz, Á. I., Terlevich, E., & Terlevich, R. 2006, MNRAS, 372, 293

Henry, R. B. C., Edmunds, M. G., Köppen, J. 2000, ApJ, 541

Isobe, T., Feigelson, E. D., Akritas, M. G., & Babu, G. J. 1990, ApJ, 364, 104

Izotov, Y. I., Chaffee, F. H., Foltz, C. B., Green, R. F., Guseva, N. G., & Thuan, T. X. 1999,

Izotov, Y. I., Chaffee, F. H., & Green, R. F. 2001, ApJ, 562, 727

Izotov, Y. I., Lipovetsky, V. A., Chaffee, F. H., Foltz, C. B., Guseva, N. G., & Kniazev, A. Y. 1997, ApJ, 476, 698

Izotov, Y. I., Papaderos, P., Guseva, N. G., Fricke, K. J., & Thuan, T. X. 2004, A&A, 421, 539

Izotov, Y. I., & Thuan, T. X. 1998, ApJ, 497, 227

Izotov, Y. I., & Thuan, T. X. 2004, ApJ, 602, 200

Kauffmann G., et al., 2003, MNRAS, 341, 33

Kehrig C., Telles E., Cuisinier F., 2004, AJ, 128, 1141

Kewley L. J., Dopita M. A., 2002, ApJS, 142, 35

Kewley, L.J., Dopita, M.A., Sutherland, R.S., Heisler, C.A., Trevena, J., 2001, ApJ, 556, 221

Kewley L. J., Ellison S. L., 2008, ApJ, 681, 1183

Kewley, L.J., Groves, B., Kauffmann, G. & Heckman, T., 2006, MNRAS, 372, 961

Kniazev, A. Y., Grebel, E. K., Hao, L., Strauss, M. A., Brinkmann, J., & Fukugita, M. 2003, ApJL, 593, L73

Lamareille F., Mouhcine M., Contini T., Lewis I., Maddox S., 2004, MNRAS, 350, 396

Lee, J. C., Salzer, J. J., & Melbourne, J. 2004, ApJ, 616, 752

Mallery R. P., et al., 2007, ApJS, 173, 482

Melbourne, J., Phillips, A., Salzer, J. J., Gronwall, C., & Sarajedini, V. L. 2004, AJ, 127, 686

Meynet, G. & Maeder, A., 2005, MNRAS, 377, 1195.

Mollá M., Vílchez J. M., Gavilán M., Díaz A. I., 2006, MNRAS, 372, 1069

Pagel, B.E.J., Edmunds, M.G., Blackwell, D.E., Chun, M.S., Smith, G. 1979, MNRAS, 189, 95

Pauldrach, A.W.A., Hoffmann, T.L. & Lennon, M. 2001, A&A, 375, 161.

Pérez-Montero, E. & Díaz, A.I. 2003, MNRAS, 346, 105

Pérez-Montero, E., & Díaz, A. I. 2005, MNRAS, 361, 1063

Pettini M., Pagel B. E. J., 2004, MNRAS, 348, L59 (PP04)

Renzini, A., Voli, M. 1981, A&A, 94, 175

Sabbadin, F., Minello, S., Bianchini, A., 1977, A&A, 60, 147

Shaw, R. A., & Dufour, R. J. 1995, PASP, 107, 896

Storchi-Bergmann T., Calzetti D., Kinney A. L., 1994, ApJ, 429, 572

Tremonti, C. A., et al. 2004, ApJ, 613, 898

Thurston, T.R., Edmunds, M.G. & Henry, R.B.C., 2996, MNRAS, 293, 990

Van Zee, L. 2000, ApJL, 543, L31

Van Zee, L., Skillman, E.D., Salzer, J.J., 1998, AJ, 116, 1186

Vermeij, R., Damour, F., van der Hulst, J. M., & Baluteau, J.-. P. 2002, A&A, 390, 649

Viironen, K., Delgado-Inglada, G., Mampaso, A., Magrini, L, Corradi, R.L.M., 2007, MNRAS, 381, 1719